The Optimal Design of Real Time Control Precision of Planar Motor

Guangdou Liu [1], Yanzhe Wang [1], Xingping Xu [1], Wuyi Ming [2], and Xin Zhang [1]

[1] College of Mechanical and Electronic Engineering
China University of Petroleum, Qingdao 266580, China
gdliu@upc.edu.cn, shidajizi212@ 163.com, xuxp@upc.edu.cn, zxin0927@163.com

[2] Department of Electromechanical Science and Engineering
Zhengzhou University of Light Industry, Zhengzhou, 450002, China
mingwuyi81@gmail.com

Abstract ─ In this paper, the Halbach permanent magnet array with 2 segments per pole is selected for analysis. The harmonics that the harmonic numbers for the ^{l}x- and ^{l}y-direction in local coordinate system are equal to each other are set as a pair for transformation. Then the expressions of the magnetic flux density distribution of the Halbach array in global coordinate system are derived. The dimensions of the coil are parameterized. The force and torque exerted on the Halbach array by a coil are calculated by Lorentz force law. The first three harmonics are chosen for real time control by analyzing the ratio of each harmonic in the total harmonics. The harmonic model has good performance on torque by comparing with the models used before. As for the force, the errors can be significantly reduced by optimizing the parameterized dimensions of coil because of the cosine or sine form error figures. The optimized model has good precision on both force and torque. The same method can be applied on the Halbach permanent magnet array with different segments per pole.

Index Terms ─ Force ripple, genetic algorithm, Halbach array, harmonic model, planar motor.

I. INTRODUCTION

The planar motor has an advantage in that the motor occupies a small area and the system can be compact in contrast to systems using two linear motors, and the planar motor is gradually applied in pick-and-place machines, lithography and inspection systems and objects which are positioned and moved in a horizontal plane [1-10]. In the planar motors, the synchronous permanent magnet planar motors with Halbach array are discussed in this paper. This type of planar motor has the advantages such as large motion, high response speed and high position precision.

Compter [6] described an electro-dynamic planar motor with moving coils and Halbach permanent array. The coils are positioned 45° relative to the Halbach permanent magnet array in this proposed planar motor. Then the arrangement of coils and Halbach array is used in the force and torque calculation. There are three models of Halbach array as follows, surface charge model, harmonic model and analytical model used in [7,8] by Jansen. To satisfy the real time control, the analytical model is applied to calculate the force and torque. There are three models of coil are presented in [7, 9]. For the calculation accuracy of the force and torque, the coil model with filaments is not taken into account. Jansen *et al*. [7] obtained the force and torque by Lorentz force law with the analytical model and coil model with surfaces. Peng *et al*. [9] calculated by the composite numerical integration and the Newton-Leibniz formula with the analytical model and coil model with surfaces and corners.

In this paper, to obtain high accuracy of force and torque exerted on the Halbach array by coil in the real time control, the harmonic model and coil model with volumes are introduced to the force and torque calculation. The coil model with volumes is optimized by Matlab with genetic algorithm toolbox [11]. The high accuracy of force and torque can be obtained when the force and torque expressions are associated with the different dimensions of coil model with volumes.

The Halbach array with 2 segments per pole shown in Fig. 1 is used in this paper. The force and torque expressions can be also applied in the Halbach array with different segments per pole, such as the Halbach array with 4 segments per pole proposed by Min *et al*. [10].

II. MODELING OF THE HALBACH ARRAY AND COIL

A. Magnetic flux density distribution in global coordinate system

Figure 1 shows the front and top view of the Halbach array with 2 segments per pole and a rectangular coil in global coordinate system. The planar motor

Submitted On: June 5, 2017
Accepted On: August 12, 2017

system is simplified by leaving out other appurtenance except for the Halbach array and a rectangular coil. The local and global coordinate systems shown in Fig. 1 are located at the center of the Halbach array. The local coordinate system is denoted with superscript ^{l} and rotates 45° clockwise about the ^{l}z-axes to get the global coordinate system. The arrows mean the magnetization direction of magnets from *s*-pole to *n*-pole, in which *N* shows the direction outward the paper and *S* toward the paper.

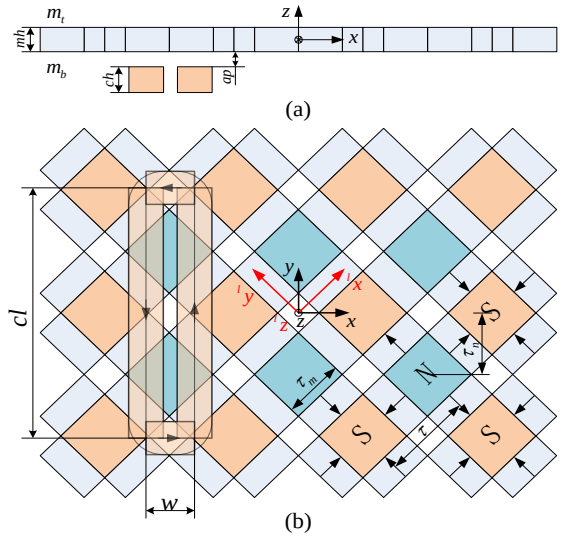

Fig. 1. The Halbach array and a rectangular coil in global coordinate system: (a) front view and (b) top view.

The expressions of the magnetic flux density distribution of the Halbach array for calculation in the local coordinate system are given by [7]:

$$ {}^{l}\vec{B} = -\sum_{m=1}^{\infty}\sum_{n=1}^{\infty} A \begin{bmatrix} m\omega\cos\left(m\omega\,{}^{l}x\right)\sin\left(n\omega\,{}^{l}y\right) \\ n\omega\sin\left(m\omega\,{}^{l}x\right)\cos\left(n\omega\,{}^{l}y\right) \\ \lambda\sin\left(m\omega\,{}^{l}x\right)\sin\left(n\omega\,{}^{l}y\right) \end{bmatrix}, \quad (1) $$

where *m* and *n* are the harmonic numbers for the ^{l}x- and ^{l}y-direction, respectively, μ_0 is the permeability, and,

$$ A = \mu_0 K_3 e^{\lambda z}, \quad (2) $$

$$ \omega = \pi/\tau, \quad (3) $$

$$ a(m) = \frac{4}{m\pi}\cos\frac{m\omega\tau_m}{2}\sin\frac{m\pi}{2}, \quad (4) $$

$$ b(m) = \frac{4}{m\pi}\sin\frac{m\omega\tau_m}{2}\sin\frac{m\pi}{2}, \quad (5) $$

$$ \lambda = \omega\sqrt{m^2+n^2}, \quad (6) $$

$$ K_3(\mu_r=1) = \frac{B_r}{2\lambda^2\mu_0}\left(e^{-m_t\lambda}-e^{-m_b\lambda}\right)\times \left(b(m)b(n)\lambda + a(m)b(n)m\omega + a(n)b(m)n\omega\right), \quad (7) $$

where τ is the pole pitch, τ_m is the length of the side of the magnets which are magnetized in ^{l}z-direction, μ_r is the relative permeability, B_r is the residual magnetization of the permanent magnet, m_t and m_b are the upper and bottom boundaries of the Halbach array, respectively.

For the expressions derived by Fourier series of magnetic flux density distribution of the Halbach array with different segments per pole, only the amplitude constant K_3 is different according the reference [15], so are the force and torque expressions derived by the magnetic flux density distribution.

The $a(m)$ and $b(m)$ are equal to zero when the *m* is even, the items only remain when *m* is an odd number. The harmonics which the harmonic numbers for the ^{l}x- and ^{l}y-direction in local coordinate system are equal to each other are set as a pair for transformation, and divided into two parts, such as m=n and m=1, n=3 (m=3, n=1). The expressions of magnetic flux density distribution of the Halbach array in the global coordinate system results in:

$$ B_x = -\frac{1}{2}\sum_{m=n=1}^{\infty} A\omega_1\sin(\omega_1 x) - \sum_{m=1}^{m<n}\sum_{n=3}^{\infty} A\sum_{i=1}^{2}(-1)^{i-1}\omega_i\sin(\omega_i x)\cos(\omega_{3-i}y), \quad (8) $$

$$ B_y = \frac{1}{2}\sum_{m=n=1}^{\infty} A\omega_1\sin(\omega_1 y) + \sum_{m=1}^{m<n}\sum_{n=3}^{\infty} A\sum_{i=1}^{2}(-1)^{i-1}\omega_i\sin(\omega_{3-i}x)\cos(\omega_3 y), \quad (9) $$

$$ B_z = \frac{1}{2}\sum_{m=n=1}^{\infty} A\lambda\left(\cos(\omega_1 x)-\cos(\omega_1 y)\right) + \sum_{m=1}^{m<n}\sum_{n=3}^{\infty} A\lambda\sum_{i=1}^{2}(-1)^{i-1}\cos(\omega_i x)\cos(\omega_{3-i}y), \quad (10) $$

where

$$ \omega_1 = \omega(m+n)/\sqrt{2}, \quad (11) $$

$$ \omega_2 = \omega(m-n)/\sqrt{2}. \quad (12) $$

B. Parameterized coil model

Figure 2 shows the coil models with volumes and the parameterized dimensions definition. There are four straight segments in coil model with volumes.

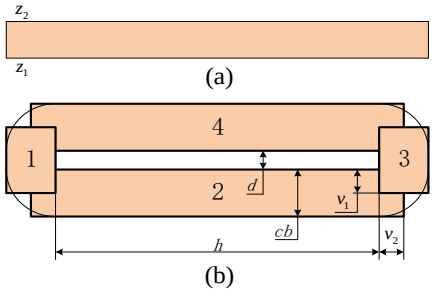

Fig. 2. The parameterized dimensions of coil with volumes: (a) front view and (b) top view.

The variables v_1 and v_2 are introduced for denoting the straight segments of coil. So the dimensions of the straight segments of the coil are not constant and can be variable for the force and torque optimization.

III. CALCULATION OF FORCE AND TORQUE

The Lorentz force and torque volume integral is applied in the force and torque calculation. The current is constant in each straight segment. The integral for the force and torque exerted on the Halbach array by one coil are equal to [14]:

$$\begin{aligned}\vec{F} &= -\int_{Vcoil} \vec{j}\times\vec{B}dV = \\ &-\int_{z_1}^{z_2}\int_{y_c-y_2}^{y_c-y_3}\int_{x_c-x_1}^{x_c+x_1}\begin{bmatrix} j & 0 & 0\end{bmatrix}^{\mathrm{T}}\times\vec{B}dxdydz \\ &-\int_{z_1}^{z_2}\int_{y_c-y_1}^{y_c+y_1}\int_{x_c+x_3}^{x_c+x_2}\begin{bmatrix} 0 & j & 0\end{bmatrix}^{\mathrm{T}}\times\vec{B}dxdydz \\ &-\int_{z_1}^{z_2}\int_{y_c+y_3}^{y_c+y_2}\int_{x_c-x_1}^{x_c+x_1}\begin{bmatrix} -j & 0 & 0\end{bmatrix}^{\mathrm{T}}\times\vec{B}dxdydz \\ &-\int_{z_1}^{z_2}\int_{y_c-y_1}^{y_c+y_1}\int_{x_c-x_2}^{x_c-x_3}\begin{bmatrix} 0 & -j & 0\end{bmatrix}^{\mathrm{T}}\times\vec{B}dxdydz\end{aligned} \quad (13)$$

$$\begin{aligned}\vec{T} &= -\int_{Vcoil} \vec{x}\times\left(\vec{j}\times\vec{B}\right)dV = \\ &-\int_{z_1}^{z_2}\int_{y_c-y_2}^{y_c-y_3}\int_{x_c-x_1}^{x_c+x_1}\vec{x}\times\left(\begin{bmatrix} j & 0 & 0\end{bmatrix}^{\mathrm{T}}\times\vec{B}\right)dxdydz \\ &-\int_{z_1}^{z_2}\int_{y_c-y_1}^{y_c+y_1}\int_{x_c+x_3}^{x_c+x_2}\vec{x}\times\left(\begin{bmatrix} 0 & j & 0\end{bmatrix}^{\mathrm{T}}\times\vec{B}\right)dxdydz \\ &-\int_{z_1}^{z_2}\int_{y_c+y_3}^{y_c+y_2}\int_{x_c-x_1}^{x_c+x_1}\vec{x}\times\left(\begin{bmatrix} -j & 0 & 0\end{bmatrix}^{\mathrm{T}}\times\vec{B}\right)dxdydz \\ &-\int_{z_1}^{z_2}\int_{y_c-y_1}^{y_c+y_1}\int_{x_c-x_2}^{x_c-x_3}\vec{x}\times\left(\begin{bmatrix} 0 & -j & 0\end{bmatrix}^{\mathrm{T}}\times\vec{B}\right)dxdydz\end{aligned} \quad (14)$$

where x_c and y_c are the x- and y-positions of the coil geometric center, respectively, and,

$$x_1 = d/2 + v_1, \quad (15)$$

$$x_2 = d/2 + cb, \quad (16)$$

$$x_3 = d/2, \quad (17)$$

$$y_1 = h/2 + v_2, \quad (18)$$

$$y_2 = h/2 + cb, \quad (19)$$

$$y_3 = h/2, \quad (20)$$

$$z_1 = m_b - ap - ch, \quad (21)$$

$$z_2 = m_b - ap, \quad (22)$$

where d and h are the width and the length of center space in the coil, respectively, ch is the height of the magnet and coil, ap is the clearance between the Halbach array and coil, cb is the bundle width of the conductor.

For the accuracy and theoretical analysis, the harmonic model and the coil model with volumes is applied to the calculation of the force and torque exerted on the Halbach array by a coil. The force and torque expressions of the coil are described as:

$$\begin{aligned}F_x &= -y_1\sum_{m=n=1}^{\infty} R_0 g(\omega_1, w)\sin(\omega_1 x) \\ &+\sum_{m=1}^{m<n}\sum_{n=3}^{\infty} R_1\sum_{i=1}^{2}\begin{pmatrix}(-1)^i g(\omega_i, w)\sin(\omega_{3-i} y_1) \\ \sin(\omega_i x)\cos(\omega_{3-i} y)\end{pmatrix},\end{aligned} \quad (23)$$

$$\begin{aligned}F_y &= x_1\sum_{m=n=1}^{\infty} R_0 g(\omega_1, cl)\sin(\omega_1 y) \\ &+\sum_{m=1}^{m<n}\sum_{n=3}^{\infty} R_1\sum_{i=1}^{2}\begin{pmatrix}(-1)^i g(\omega_{3-i}, cl)\sin(\omega_i x_1) \\ \cos(\omega_i x)\sin(\omega_{3-i} y)\end{pmatrix},\end{aligned} \quad (24)$$

$$\begin{aligned}F_z &= \sum_{m=n=1}^{\infty} R_0\begin{pmatrix}y_1 g(\omega_1, w)\cos(\omega_1 x) \\ -x_1 g(\omega_1, cl)\cos(\omega_1 y)\end{pmatrix} \\ &+\sum_{m=1}^{m<n}\sum_{n=3}^{\infty}\frac{R_1}{\lambda}\sum_{i=1}^{2}\begin{pmatrix}(-1)^i\begin{pmatrix}\omega_{3-i} g(\omega_{3-i}, w)\sin(\omega_i y_1) \\ +\omega_i g(\omega_i, cl)\sin(\omega_{3-i} x_1)\end{pmatrix} \\ \cos(\omega_{3-i} x)\cos(\omega_i y)\end{pmatrix},\end{aligned} \quad (25)$$

$$\begin{aligned}T_x &= F_y(C_2) - yF_z - x_1\sum_{m=n=1}^{\infty}\frac{R_0}{2}h(\omega_1, cl)\sin(\omega_1 y) \\ &+\sum_{m=1}^{m<n}\sum_{n=3}^{\infty}\frac{R_1}{2\lambda}\sum_{i=1}^{2}\begin{pmatrix}\frac{(-1)^i}{\omega_i}\begin{pmatrix}2\omega_{3-i} g(\omega_{3-i}, w)u(\omega_i, y_1) \\ +\omega_i^2 h(\omega_i, cl)\sin(\omega_{3-i} x_1)\end{pmatrix} \\ \cos(\omega_{3-i} x)\sin(\omega_i y)\end{pmatrix},\end{aligned} \quad (26)$$

$$\begin{aligned}T_y &= xF_z - F_x(C_2) - y_1\sum_{m=1}^{\infty}\frac{R_0}{2}h(\omega_1, w)\sin(\omega_1 x) + \\ &\sum_{m=1}^{m<n}\sum_{n=3}^{\infty}\frac{R_1}{2\lambda}\sum_{i=1}^{2}\begin{pmatrix}\frac{(-1)^i}{\omega_i}\begin{pmatrix}2\omega_{3-i} g(\omega_{3-i}, cl)u(\omega_i, x_1) \\ +\omega_i^2 h(\omega_i, w)\sin(\omega_{3-i} y_1)\end{pmatrix} \\ \sin(\omega_i x)\cos(\omega_{3-i} y)\end{pmatrix},\end{aligned} \quad (27)$$

$$\begin{aligned}T_z &= -xF_y + yF_x + \\ &\sum_{m=1}^{m<n}\sum_{n=3}^{\infty}\frac{R_1}{\omega_1\omega_2}\sum_{i=1}^{2}\begin{pmatrix}(-1)^i\begin{pmatrix}\omega_{3-i} g(\omega_{3-i}, cl)u(\omega_i, x_1) \\ -\omega_i g(\omega_i, w)u(\omega_{3-i}, y_1)\end{pmatrix} \\ \sin(\omega_i x)\sin(\omega_{3-i} y)\end{pmatrix},\end{aligned} \quad (28)$$

where

$$g(\omega_i, cl) = \sin\frac{\omega_i w}{2}\sin\frac{\omega_i cb}{2}, \quad (29)$$

$$\begin{aligned}h(\omega_i, cl) &= \frac{cl}{2}\cos\frac{\omega_i cl}{2}\sin\frac{\omega_i cb}{2} + \\ &\frac{cb}{2}\sin\frac{\omega_i cl}{2}\cos\frac{\omega_i cb}{2} - \frac{2}{\omega_i}\sin\frac{\omega_i cl}{2}\sin\frac{\omega_i cb}{2}\end{aligned}, \quad (30)$$

$$u(\omega_i, y_1) = \omega_i y_1\cos(\omega_i y_1) - \sin(\omega_i y_1), \quad (31)$$

$$C_1 = \left(e^{\lambda z_2} - e^{\lambda z_1}\right)/\lambda, \quad (32)$$

$$C_2 = \left(e^{\lambda z_1} - e^{\lambda z_2} + \lambda z_2 e^{\lambda z_2} - \lambda z_1 e^{\lambda z_1}\right)/\lambda^2, \quad (33)$$

$$R_0 = 4 j\mu_0 K_3 C_1, \quad (34)$$

$$R_1 = 8 j\mu_0 K_3\lambda C_1/(\omega_1\omega_2), \quad (35)$$

and *w* and *cl* are the sizes of the filament coil along the *x*- and *y*-directions, respectively, $F_y(C_2)$ and $F_x(C_2)$ mean the C_1 is only replaced by C_2 in the F_x and F_y expressions without changing the others, respectively.

IV. COMPARISON OF FORCE AND TORQUE

The force and torque expressions of the harmonic model and coil model with volumes are too complicated to be used in real time control and can be simplified by analyzing the ratio of each harmonic. Figure 3 shows the ratio of each harmonic in the total harmonics. It is found that the ratios of each higher harmonic decrease along the air-gap length in *z*-direction. The majority harmonics are composed of *m*=1, *n*=1, *m*=1, *n*=3 and *m*=3, *n*=1. The maximum ratio magnitudes of m=1, n=5 and m=5, n=1 along the air-gap length in *z*-direction are 0.627%. So the force and torque expressions are simplified by taking the first three harmonics in the real time control and the others can be ignored due to the ratio magnitudes.

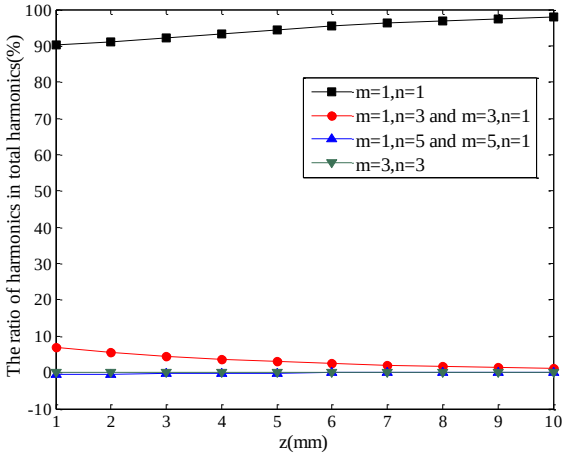

Fig. 3. Ratio of harmonic in total harmonics along the air-gap length in *z*-direction.

In the real time control, the calculation time is an important item to be inspected. Take the force F_x for example, the simplified expression is list as follow:

$$F_x = C_{x1}\sin\left(\sqrt{2}\omega x\right) + C_{x2}\sin\left(2\sqrt{2}\omega x\right)\cdot \cos\left(\sqrt{2}\omega y\right) + C_{x3}\sin\left(\sqrt{2}\omega x\right)\cos\left(2\sqrt{2}\omega y\right), \quad (36)$$

where

$$C_{x1} = -y_1\left(R_0 g\left(\omega_1, w\right)\right)_{(1,1)}, \quad (37)$$

$$C_{x2} = \sin\left(\sqrt{2}\omega y_1\right)\left(R_1 g\left(\omega_1, w\right)\right)_{(1,3)}, \quad (38)$$

$$C_{x3} = -\sin\left(2\sqrt{2}\omega y_1\right)\left(R_1 g\left(\omega_2, w\right)\right)_{(1,3)}, \quad (39)$$

and the coefficient C_{x1} is calculated with the subscript (1,1) denoting *m*=1 and *n*=1, so do the C_{x2} and C_{x3}.

The other force and torque expressions are similar to F_x and not list. The calculation time is determined on the DSP system. The simplified force and torque also have simple expressions to get short calculation time.

The same dimensions of coil and Halbach array to the planar motor used by Jansen are adopted. The variables v_1 and v_2 take 4.75 mm and 4.75 mm for the consistency with the model used by Jansen, respectively. Then the x_1 and y_1 are equal to 6.65 mm and 35.95 mm, respectively. The parameters of coil and Halbach array are shown in Table 1.

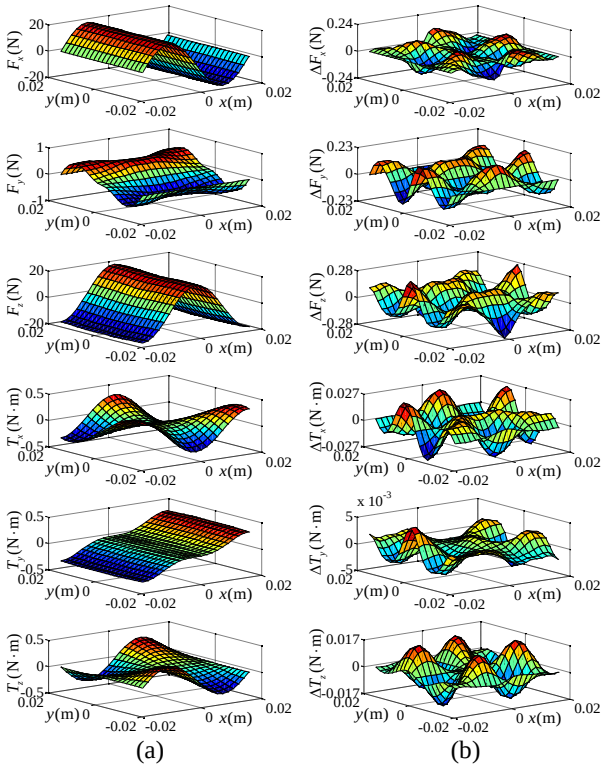

Fig. 4. (a) The force and torque predictions by Ansoft Maxwell, and (b) the force and torque error predictions between the model used by Peng and Ansoft Maxwell.

Table 1: Parameters of coil and Halbach array

Parameters	Value	Unit
Pole pitch (τ)	25	mm
Position of the top of the array (m_t)	3.5	mm
Position of the bottom of the array (m_b)	-3.5	mm
Clearance (ap)	1	mm
Coil length (cl)	71.9	mm
Coil width (w)	13.3	mm
Conductor bundle width (cb)	9.5	mm
Magnet size ratio (τ_m/τ)	0.68	-
Remanence of the magnets (B_r)	1.24	T
Current density (j)	10	A/mm^2

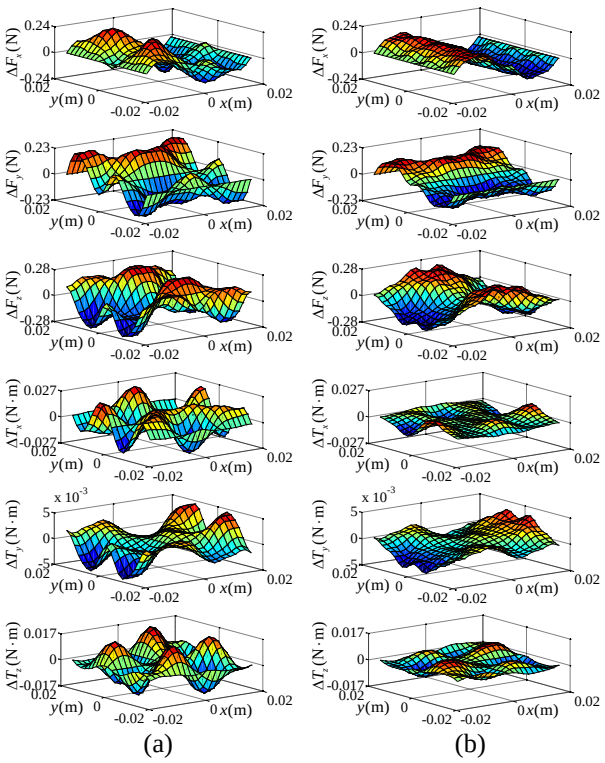

Fig. 5. The force and torque error predictions: (c) between the model used by Jansen and Ansoft Maxwell, and (d) between the model proposed by this paper and Ansoft Maxwell.

To validate the accuracy, the force and torque calculated by Ansoft Maxwell [12], Jansen, Peng and this paper are compared. Jansen used the analytical model and coil model with surfaces, Peng used the analytical model and coil model with surfaces and corners. The force and torque predictions are compared for the positions of the center of coil in a square region, which is located at z = -7.5 mm, with x from -17.7 mm to 17.7 mm and y from -17.7 mm to 17.7 mm. The square region shows a period in Halbach array and is split into 21×21 points, each of which is the coordinate values of the center of coil.

The force and torque predictions by Ansoft Maxwell and the force and torque error predictions between the model used by Peng and Ansoft Maxwell are shown in Fig. 4. The force and torque error predictions between the model used by Jansen and Ansoft Maxwell and between the model proposed by this paper and Ansoft Maxwell are shown in Fig. 5.

From Fig. 4 and Fig. 5, it is difficult to distinguish which is best in the force and torque calculation. The root mean square (rms) value which represents the ripples of the force and torque is introduced to predict the performance of the error predictions for each model. The smaller of the rms value, the better of the model. The rms values of the errors of the model used by Peng, the model used by Jansen and the model proposed by this paper are shown in Table 2.

Table 2: Parameters of each model

Parameters	Model used by Peng	Model used by Jansen	Model Proposed by this Paper	Unit
rms (ΔF_x)	0.0506	0.1022	0.0928	N
rms (ΔF_y)	0.0803	0.116	0.0884	N
rms (ΔF_z)	0.0990	0.159	0.1316	N
rms (ΔT_x)	0.0107	0.0111	0.0037	Nm
rms (ΔT_y)	0.0015	0.0019	0.0014	Nm
rms (ΔT_z)	0.0071	0.0073	0.0030	Nm

It can be seen in Table 2, the accuracy of the model used by Peng is best in the rms values of the force components and the accuracy of the model used by this paper is best in the rms values of the torque components. From the Fig. 5 (b), the three components of the force error predictions are close to cosine or sine form. According to the force predictions of Ansoft Maxwell and the error predictions between the model proposed by this paper and Ansoft Maxwell, the force error can be significantly reduced by optimizing the parameterized dimensions of coil.

V. OPTIMIZATION OF FORCE AND TORQUE

In order to reduce the force and torque error, the model proposed by this paper is optimized by genetic algorithm (GA).

The objective function is the maximum error of each force and torque components between the model proposed by this paper and Ansoft Maxwell on coil center coordinates in the square region mentioned above. The function is given by:

$$f(x_1, y_1) = \max\left|R_1(S_{mn}) - R_2(S_{mn})\right|, \quad (40)$$

where R_1 and R_2 are the force and torque obtained by Ansoft Maxwell and the model proposed by this paper, respectively, the function R represents F_x, F_y, F_z, T_x, T_y and T_z, respectively, S_{mn} is the coordinate values of coil center, in which the values are in millimeters, and,

$$S_{mn} = (-17.7 + 1.77m, -17.7 + 1.77n, -7.5). \quad (41)$$

There are two parameters x_1 and y_1 by observing the force and torque expressions, which are related to the v_1 and v_2, respectively. In this part, the parameters x_1 and y_1 are set as variables for optimizing the force and torque. The optimization variables are shown in Table 3.

In the optimization of torque, the values of the F_x, F_y and F_z in the torque expressions are considered as constant obtained by the force optimization before. So the dimensions of x_1 and y_1 used in force and torque are different. The flowchart of the parameter optimizing

procedure using genetic algorithm (GA) [13] is shown in Fig. 6. The genetic algorithm of optimization tool of MATLAB is used. Firstly, the elite are selected by fitness evaluation. Then the new elite are selected from the new population generated by the crossover and mutation. Finally, the stopping criterion is the stall generations reach one hundred. The selection function, crossover function and mutation function use stochastic uniform, scattered and use constraint dependent, respectively.

Table 3: Optimization variables

Variables	Constraints	Unit
The dimension of the coil straight segments in x-direction (x_1)	$\left[\frac{d}{2}, \frac{d}{2}+cb\right]$	mm
The dimension of the coil straight segments in y-direction (y_1)	$\left[\frac{h}{2}, \frac{h}{2}+cb\right]$	mm

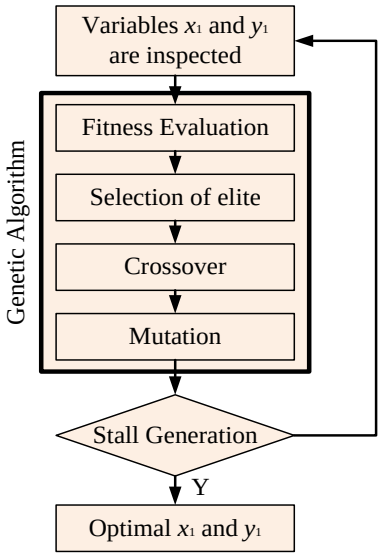

Fig. 6. The optimization process.

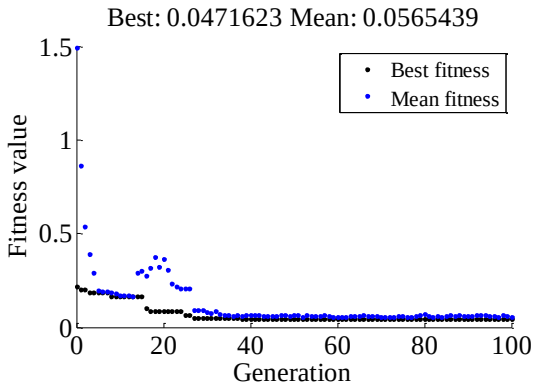

Fig. 7. Iteration accomplished by GA to obtain the best fitness for *Fz*.

The fitness values of F_z shown in Fig. 7, illustrate that after 40 number of iteration the error reaches to an acceptable value. The other force and torque are similar and not listed. The results of the optimization variables are shown in Table 4.

Table 4: The results of the optimization variables

Force and Torque	x_1 (mm)	y_1 (mm)	$f(x_1, y_1)$
F_x (N)	-	36.2	0.1761
F_y (N)	8.69	-	0.0093
F_z (N)	8.34	36.2	1.4763
T_x (Nm)	6.84	31.53	0.0440
T_y (Nm)	7.14	36.9	0.0195
T_z (Nm)	11.4	38.12	0.0019

The error predictions between the optimized model and Ansoft Maxwell are shown in Fig. 8. Each error prediction is obtained by using the different optimization results. The rms values of the error between the optimized model and Ansoft Maxwell are shown in Table 5.

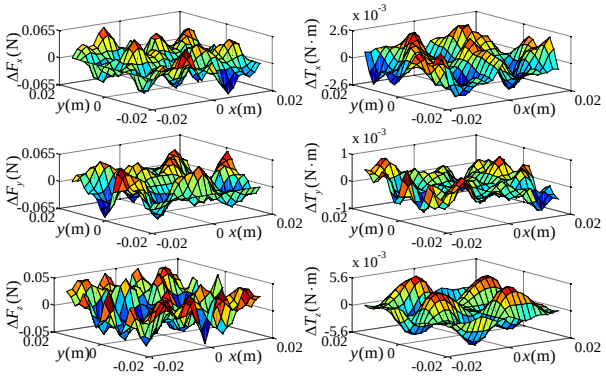

Fig. 8. Error predictions after optimization of the force exerted by a coil.

Table 5: The rms values of the error between the optimized model and Ansoft Maxwell

Parameters	Optimized	Unit
rms (ΔF_x)	0.0228	N
rms (ΔF_y)	0.0254	N
rms (ΔF_z)	0.0249	N
rms (ΔT_x)	0.0011	Nm
rms (ΔT_y)	0.0003	Nm
rms (ΔT_z)	0.0006	Nm

Comparing the force rms values of the optimized model with the model used by Peng, the rms values are much lower. The rms (ΔF_x), rms (ΔF_y) and rms (ΔF_z) are 45.06%, 31.63% and 25.15% of the model used by Peng, respectively. Comparing the torque rms values of the optimized model with the model proposed by this paper, the lower rms values are obtained. The rms (ΔT_x),

rms (ΔT_y) and rms (ΔT_z) are 29.73%, 21.43% and 20% of the model proposed by this paper, respectively. The only change between the optimized model and the model proposed by this paper is that different dimensions of coil segments are adopted for force and torque calculation. The optimized model can achieve good accuracy.

VI. CONCLUSION

The magnetic flux density distribution of the Halbach array is expressed in global coordinate system after transformation. The dimensions of coil are parameterized for modeling.

The analytical expressions of force and torque exerted on the Halbach array by a coil with the harmonic model and the coil model with volumes are obtained. The model proposed by this paper is simplified by taking the first three harmonics to be used in real time control.

The rms for force and torque of the optimized model are very low comparing with the previous models. The optimized model can be applied to the force and torque calculation to improve control precision. The same method can be applied on the Halbach permanent magnet array with different segments per pole.

ACKNOWLEDGMENT

Research was supported by the Natural Foundation of Shandong Province (ZR2015EQ015) and the Fundamental Research Funds for the Central Universities (15CX02031A, 15CX02123A).

REFERENCES

[1] H. S. Cho and H. K. Jung, "Analysis and design of synchronous permanent-magnet planar motors," *IEEE Trans. Energy Conver.*, vol. 17, no. 4, pp. 492-499, 2002.

[2] A. Shiri and A. Shoulaie, "Investigation of frequency effects on the performance of single-sided linear induction motor," *Applied Computational Electromagnetics Society (ACES) Journal*, vol. 27, no. 6, pp. 497-504, June 2012.

[3] J. F. Pan, N. C. Cheung, and J. M. Yang, "High-precision position control of a novel planar switched reluctance motor," *IEEE Trans. Ind. Electron.*, vol. 52, no. 6, pp. 1644-1652, Dec. 2005.

[4] H.-S. Cho and H.-K. Jung, "Analysis and design of synchronous permanent-magnet planar motors," *IEEE Trans. Energy Convers.*, vol. 17, no. 4, pp. 492-499, Dec. 2002.

[5] L. Huang, X. Huang, H. Jiang, and G. Zhou, "Comparative study of magnetic fields due to types of planar permanent magnet array," *International Conference on Electrical and Control Engineering*, DOI 10. 1109/Icece. 844, 2010.

[6] J. C. Compter, "Electro-dynamic planar motor," *Precision Eng.*, vol. 28, pp. 171-180, 2004.

[7] J. W. Jansen, C. M. M. van Lierop, E. A. Lomonova, and A. J. A. Vandenput, "Modeling of magnetically levitated planar actuators with moving magnets," *IEEE Trans. Magn.*, vol. 43, no. 1, pp. 15-25, Jan. 2007.

[8] J. W. Jansen, C. M. M. van Lierop, E. A. Lomonova, and A. J. A. Van-denput, "Magnetically levitated planar actuator with moving magnets," *in Proc. IEEE Int. Electric Machines & Drives Conf.* (IEMDC '07), vol. 1, pp. 272-278, May 2007.

[9] J. Peng, Y. Zhou, and G. Lin, "Calculation of a new real-time control model for the magnetically levitated ironless planar motor," *IEEE Trans. Magn.*, vol. 49, no. 4, pp. 1416-1422, Jan. 2013.

[10] W. Min, M. Zhang, Y. Zhu, B. Chen, G. Duan, J. Hu, and W. Yin, "Analysis and optimization of a new 2-D magnet array for planar motor," *IEEE Trans. Magn.*, vol. 46, no. 5, May 2010.

[11] Numerical Integration and Differentiation Users Guide [M]. Mathworks Inc., 2009.

[12] E. Schmidt and M. Hofer, "Application of the sliding surface method with 3D finite element analyses of a hybrid magnetic bearing," *25th Annual Review of Progress in Applied Computational Electromagnetics (ACES)*, Monterey, California, pp. 440-445, Mar. 2009.

[13] A. Nejadpak, M. R. Barzegaran, and O. A. Mohammed, "Evaluation of high frequency electromagnetic behavior of planar inductor designs for resonant circuits in switching power converters," *Applied Computational Electromagnetics Society Journal*, vol. 26, no. 9, pp. 737-748, 2011.

[14] K. J. Binns, P. J. Lawrenson, and C. W. Towbridge, *The Analytical and Numerical Solutions of Electrical and Magnetic Fields*. Chichester, England: *John Wiley & Sons*, 1994.

[15] Y. Zhou, G. Liu, R. Zhou, L. Huo, and W. Ming, "Modeling and comparison of the Halbach array with different segments per pole," *International Journal of Applied Electromagnetics and Mechanics*, vol. 47, no. 3, pp. 629-641, 2015.